



Periodicity Search for Pulsar Binaries with TESS

Partha Sarathi Pal¹, P. H. T. Tam¹, Weitang Liang¹, Chengye Cao¹, K. L. Li², C. Y. Hui³, and A. K. H. Kong²

¹School of Physics and Astronomy, Sun Yat Sen University, Guangzhou 510275, People's Republic of China; tanbxuan@mail.sysu.edu.cn

²Institute of Astronomy, National Tsing Hua University, Hsinchu 30013, Taiwan

³Department of Astronomy & Space Science, Chungnam National University, Daejeon 34134, Republic of Korea

Received 2020 February 15; revised 2020 May 12; accepted 2020 May 14; published 2020 May 29

Abstract

Pulsar binaries, in particular redback systems, provide good sources to study the pulsar wind flow and its interaction with the companion stars. Fermi-LAT have proposed probable pulsar binary candidates in its catalogs. An orbital modulation search of binary candidates is an effective way to identify pulsar binary sources from the catalog. Transiting Exoplanet Survey Satellite (TESS) observes in survey mode for a large part of the sky and thus provides an excellent data set for the periodicity search of pulsar binary candidates by observing the flux variation, thought to mainly come from the stellar companion. Using TESS data we look for flux modulation of five pulsar binaries (or candidates) with reported orbital periods, including PSR J1023+0038, 3FGL J0523.3–2528, 3FGL J0212.1+5320, 3FGL J0744.1–2523, and PSR J1417–4402, demonstrating that TESS photometric data are very useful in identifying periodicities of redback-like systems. This method can be effective in searches for new pulsar binaries or similar binary systems in the future.

Unified Astronomy Thesaurus concepts: [Astronomy data analysis \(1858\)](#); [Binary pulsars \(153\)](#); [Pulsars \(1306\)](#)

1. Introduction

Redback systems are close-orbit pulsar binaries that show intense interactions between the pulsars and the companion stars. The orbital period of redbacks typically spans $P_b \leq 20$ hr (Roberts 2013; Hui & Li 2019), with the exception of PSR J1306–40 $P_b = 26.3$ hr (Linares 2018; Swihart et al. 2019). The companion stars are late-type nondegenerate ones with masses of $M_c \sim 0.2\text{--}0.5 M_\odot$, which are significantly higher than those of another similar class of systems, black widows, for which $M_c < 0.1 M_\odot$ (Roberts 2013; Hui & Li 2019). Some redbacks have been observed to transit between the rotation-powered state and a state with an accretion disk, such as those observed in PSR J1023+0038 and XSS J12270–4859 (see, e.g., Archibald et al. 2009; Papitto et al. 2013; Bassa et al. 2014; Patruno et al. 2014; Stappers et al. 2014; Takata et al. 2014; Roy et al. 2015, and references therein). Pulsar binaries of longer orbital periods than one day, such as PSR J1417–4402, have also been discovered (e.g., Swihart et al. 2018).

Optical periodicity related to the pulsar irradiation and ellipsoidal variation have been observed in many of the known pulsar binaries. At the same time, nonperiodic phenomena such as optical flares (e.g., from the accretion disk) and flux change (between different states/modes) at various timescales can also be used to probe the astrophysical conditions of the systems.

Transiting Exoplanet Survey Satellite (TESS) is a survey satellite with a bandpass of 600–1000 nm whose principal mission is to observe flux variation of stars to determine the presence of exoplanets around those stars (Ricker et al. 2015). With its supreme timing ability at timescales of minutes to hours and its nearly all-sky coverage, it is also an ideal instrument to characterize periodicities and flux variations of stars (Dorn-Wallenstein et al. 2019; Balona & Ozuyar 2020) and binaries, such as redbacks either in their accretion or rotation-powered states.

In this work, we searched through the literature for known redback-like pulsar binaries (or candidates) with a reported orbital period, including those covered by TESS target

products. The chosen sources are given in Table 1. The aim is to demonstrate the photometric capabilities of TESS to characterize redbacks and similar systems.

2. The Redback Systems (Candidates)

2.1. PSR J1023+0038

The prototypical redback pulsar, PSR J1023+0038, has shown transitions between a low-mass X-ray binary (LMXB) state and a rotation-powered state (see, e.g., Archibald et al. 2009; Tam et al. 2010; Patruno et al. 2014; Stappers et al. 2014). A single-humped modulation in optical for 4.75 hr was first reported in Woudt et al. (2004), during the time now believed to be a pulsar state. Time-resolved optical spectroscopy and photometry of PSR J1023+0038 revealed that it is an X-ray binary and consists of a late-type G5 companion star with a period of 4.75 hr (Thorstensen & Armstrong 2005). Subsequently, detection of a pulsar spin period of 1.69 ms in 2007 confirmed the primary as a radio millisecond pulsar (MSP; Archibald et al. 2009). Using further observations, it has been found that the donor star has a mass $M_2 \sim 0.24 M_\odot$, $M_{NS} = 1.71 \pm 0.16 M_\odot$, and the binary at a distance $d = 1.37 \pm 0.04$ kpc (Deller et al. 2012; McConnell et al. 2015). In 2013 the transition from the MSP to LMXB state of PSR J1023+0038 was reported with the disappearance of radio pulsation and the increase in optical, X-ray, and γ -ray fluxes (Patruno et al. 2014; Stappers et al. 2014; Takata et al. 2014).

Since then, in the current accretion state, PSR J1023+0038 shows rapid flickering and double-peaked emission lines in a blue optical spectrum, believed to be associated with an accretion disk (e.g., Kennedy et al. 2018; Shahbaz et al. 2019), as first seen in the previous accretion state (Szkody et al. 2003).

On 2019 February 2 20:09:35 UTC TESS observed PSR J1023+0038 for 27 days under TESS GI Proposal ID: #G011187 (PI: Mark Kennedy).

Table 1

List of Sources Analyzed: (1) Source Names, (2) Right Ascension, (3) Declination, (4) Observation Start Time, (5) Observation Stop Time, (6) Sector, (7) Camera No., (8) CCD No., (9) TESS Magnitude

| Source Name | R.A. ($^{\circ}$) (2) | Decl. ($^{\circ}$) (3) | Start Time (UTC) (4) | Stop Time (UTC) (5) | Sector (#) (6) | Camera (#) (7) | CCD (#) (8) | TESS (Mag.) (9) |
|-------------------|-------------------------------|--------------------------------|--|---|----------------------|----------------------|-------------------|-----------------------|
| PSR J1023+0038 | 155.948668 | 0.644794 | 2019 Feb 2 20:09:36 | 2019 Feb 27 11:59:35 | 8 | 1 | 3 | 16.28 |
| 3FGL J0523.3–2528 | 80.820517 | –25.460263 | 2018 Nov 15 11:25:40 2018 Dec 15 18:27:39 | 2018 Dec 11 18:53:39 2019 Jan 6 13:03:39 | 5 6 | 2 2 | 2 1 | 15.78 15.78 |
| 3FGL J0212.1+5320 | 33.043655 | 53.360771 | 2019 Nov 3 03:35:26 | 2019 Nov 27 12:43:25 | 18 | 2 | 3 | 13.85 |
| 3FGL J0744.1–2523 | 116.044700 | –25.399400 | 2019 Jan 8 02:59:37 | 2019 Feb 1 13:59:36 | 7 | 2 | 2 | ... |
| PSR J1417–4402 | 214.377517 | –44.049269 | 2019 Apr 23 06:29:33 | 2019 May 20 08:59:32 | 11 | 1 | 2 | ... |

2.2. 3FGL J0523.3–2528

1FGL J0523.5–2529 was discovered as a Fermi-LAT unidentified γ -ray source (Abdo et al. 2010), without detected radio emission yet (Guillemot et al. 2012; Petrov et al. 2013). Later it was recataloged as 3FGL J0523.3–2528 (Acero et al. 2015). The optical photometry and the Southern Astrophysical Research (SOAR) Telescope spectroscopic observations of an X-ray source detected within the localization error of 3FGL J0523.3–2528 revealed a periodic flux modulation of a 16.5 hr period (Strader et al. 2014). The radial velocity variations indicate a probable binary pulsar with an unusually massive ($0.8 M_{\odot}$) secondary companion and a measurable eccentricity ($e = 0.04$; Strader et al. 2014).

From 2018 November 15 11:25:39 UTC to 2018 December 15 18:27:39 UTC, TESS observed 3FGL J0523.3–2528 for 54 days under TESS GI Proposal ID: #G011187 (PI: Mark Kennedy).

2.3. 3FGL J0212.1+5320

3FGL J0212.1+5320 was first discovered as an unidentified γ -ray source, 1FGL J0212.3+5319 (Abdo et al. 2010). Detailed photometry and optical spectroscopy classified 3FGL J0212.1+5320 as a redback MSP candidate with a period of 0.87 days (Li et al. 2016; Linares et al. 2017). From spectroscopic modeling of 3FGL J0212.1+5320 optical data, it is reported that the 3FGL J0212.1+5320 binary system may consist of a neutron star and a secondary star mass of $M_1 = 1.85^{+0.32}_{-0.26} M_{\odot}$ and $M_2 = 0.50^{+0.22}_{-0.19} M_{\odot}$, respectively (Shahbaz et al. 2017).

On 2019 November 3 03:35:25 UTC, TESS observed 3FGL J0212.1+5320 for a 27 day exposure time under TESS GI Proposal ID: #G022055 (PI: Francesco Coti Zelati).

2.4. 3FGL J0744.1–2523

3FGL J0744.1–2523 was detected as an unidentified γ -ray source. No associated X-ray source, within 0.3–10 keV 3σ upper limit, is detected down to a limit of 4.5×10^{-14} erg s $^{-1}$ cm $^{-2}$. The field of 3FGL J0744.1–2523 is not covered by the Catalina Sky Survey. A variable Gamma-Ray Burst Optical/Near-Infrared Detector (GROND) source within the error ellipse of 3FGL J0744.1–2523 has been found. This source features a clear flux modulation with an optical and near-IR period equal to 0.115 days (Salvetti et al. 2017). We note that such a candidate optical counterpart is now outside the 4FGL error circle, and no bright radio or optical counterpart can be found within the 4FGL 95% error circle.

On 2019 January 8 02:59:36 UTC, TESS observed the 3FGL J0744.1–2523 sky location during sector #7 of its survey mode for a 27 day exposure time.

2.5. PSR J1417–4402

PSR J1417–4402 was detected as a γ -ray source by Fermi-LAT and cataloged as 3FGL J1417.5-4402 (Abdo et al. 2010). Photometric and spectroscopic analysis of the optical counterpart reported a period of 5.37 days, with no significant eccentricity, at a distance of 4.4 kpc. The mass ratio of the system is predicted around $\frac{M_2}{M_{NS}} = 0.18$. The estimated mass of the components are $M_{NS} = 1.97 \pm 0.15 M_{\odot}$ and $M_2 = 0.35 \pm 0.04 M_{\odot}$ (Strader et al. 2015). A 2.66 ms radio pulsar PSR J1417–4402 has been found and the distance from radio data is estimated to be 1.6 kpc (Camilo et al. 2016). Subsequently, PSR J1417–4402 is classified to be a redback-like system (Swihart et al. 2018; De Vito et al. 2019).

On 2019 April 23 06:29:33 UTC, TESS observed PSR J1417–4402 sky location during sector #11 of its survey mode for a 27 day exposure time.

3. Data Analysis

Periodicity searches were performed using archival TESS data. The obtained periodicity is then compared to the reported orbital periods.

The TESS archival data are searched and obtained with *Astroquery*. PSR J1023+0038, 3FGL J0523.3–2528, 3FGL J0212.1+5320 are observed under TESS Guest Investigator Program. For these three sources 2 minute cadence *timeseries* data are downloaded. For 3FGL J0744.1–2523 and PSR J1417–4402, *TESSCUT* 30 minute cadence full-frame image (FFI) data within $3'85 \times 3'85$ are downloaded. All data are analyzed with *Lightkurve* (Lightkurve Collaboration et al. 2018). Light curve files are generated with `to_lightcurve()` from calibrated target-pixel files. For GI proposal data *lightkurve* defined aperture mask `pipeline_mask` for the GI proposal data. For 3FGL J0744.1–2523 *TESSCUT* data the aperture mask is chosen manually depending upon the presence of peak profile in power density spectra (PDSs) of the individual pixels. The infinite or NaN values are excluded from light curves with `remove_nans()`. The outliers above the 3σ level in the light curves are clipped with `remove_outliers()`. The threshold for PSR J1023+0038 is set to 6σ to retain the flaring events. All cleaned unbinned light curves are plotted in the top panels of Figures 2(a)–(d). In order to search periodicities in the optical flux PDSs are generated with `to_periodogram` from cleaned unbinned light curves. PDSs are calculated using the

Table 2PDS Fitting Results: (1) Source Names, (2) Orbital Period Calculated from the Peak Frequency of the Lorentzian Profile, (3) FWHM of Lorentzian, (4) Q -value, (5) rms Amplitude (%), (6) Reduced χ^2 Value

| Source Name | Period (hr) | FWHM (hr) | Q -value | Rms (%) | χ_r^2 (dof) |
|-------------------|----------------------|---------------------|------------|------------|---------------------|
| (1) | (2) | (3) | (4) | (5) | (6) |
| PSR J1023+0038 | 4.7816 ± 0.0015 | 0.0274 ± 0.0027 | 174.57 | 19.22 | 2.17(40) |
| 3FGL J0523.3–2528 | 8.2768 ± 0.0020 | 0.0207 ± 0.0010 | 400.62 | 8.99 | 0.65(55) |
| | 16.4411 ± 0.0149 | 0.0994 ± 0.0068 | 165.42 | 2.68 | 0.12(19) |
| | 5.5028 ± 0.0037 | 0.0251 ± 0.0041 | 219.18 | 3.02 | 0.07(42) |
| 3FGL J0212.1+5320 | 10.4659 ± 0.0051 | 0.0167 ± 0.0751 | 625.48 | 15.74 | 0.08(18) |
| 3FGL J0744.1–2523 | 2.7634 ± 0.0008 | 0.0034 ± 0.0015 | 815.86 | 0.70 | 0.01(38) |

Lomb–Scargle method and normalized to the power spectral density (Balona & Ozuyar 2020). Significant peak profiles in PDSs are determined with Bayesian block analysis (Scargle et al. 2013) with 95% statistical significance using *Astropy*. The peak profiles obtained from Bayesian block analysis are fitted with a Lorentzian profile (Belloni et al. 2002) using *Scipy* to estimate the significance of the peak profiles. From the curve fitting Q -value ($\frac{\nu}{\Delta\nu}$) (Casella et al. 2005), the rms amplitude⁴ (see Equation (1)) and reduced χ^2 are calculated as the goodness of fit. The 1σ error bars are estimated from the covariance matrix. The analysis results are shown in Table 2. In the middle panel of Figures 2(a)–(d) PDSs are shown in black color. The Bayesian blocks are shown in gray dashed lines. The Lorentzian peak profiles are shown in red, green, and blue dashed lines. The continuum part of the PDSs is fitted with a power-law model and shown in the magenta dashed line as an estimation of noise in the PDSs.

$$\text{rms} = 100 \times \sqrt{\frac{A}{\text{Flux}}} \%,$$

$$\text{where, } A = \frac{\pi}{2} \times \text{Normalization} \times \text{FWHM},$$

$$= \text{Flux under Lorentzian function};$$

$$\text{Normalization} = \text{Power at peak frequency},$$

$$\text{FWHM} = \text{Full width half maxima.} \quad (1)$$

Before detailed analysis for individual sources, one would like to first verify that the obtained periodicity in the PDSs indeed comes from the corresponding redback positions. Hence, PDSs of pixels around the aperture mask (i.e., neighborhood pixels) are plotted with Bayesian blocks, as shown in Figures 1(a)–(d). In Figures 1(a)–(c) the blue boxes mark the pixels included in the pipeline-defined aperture mask. For 3FGL J0744.1–2523 in Figure 1(d), the 5×5 pixel PDS plot with peak profiles at the same frequencies are observed. The pixel with the strongest peak profile is taken as the aperture mask for the further analysis of 3FGL J0744.1–2523 TESS-CUT data (marked with a red box). For PSR J1417–4402 in Figure 3(a), the 5×5 pixel PDS plot is shown where no peak profile is observed. The pixel coordinates are projected on sky coordinates, and PSR J1417–4402 sky coordinates coincide with pixel #13, which is marked with a blue box. This pixel is taken as the aperture mask for further analysis of PSR J1417–4402 TESSCUT data.

⁴ https://heasarc.gsfc.nasa.gov/docs/xte/recipes/pca_fourier.html

With the obtained orbit-related periodicities of redback systems (candidates) using TESS data, we then fold the TESS light curves for four sources with the orbital period, as shown in the bottom panels of Figures 2(a)–(d) and 3(b). The low frequency trends are removed from data using Savitzky–Golay filter. The flux is normalized to the median flux of each source. The phase zero (T_0) is set to the inferior conjunction (when the companion is between the pulsar and the observer), following Thorstensen & Armstrong (2005) for PSR J1023+0038, Linares et al. (2017) for 3FGL J0212.1+5320, Strader et al. (2014) for 3FGL J0523.3–2528, and Salvetti et al. (2017) for 3FGL J0744.1–2523.

4. Results

4.1. PSR J1023+0038

In TESS data PSR J1023+0038 shows a median flux around $60 e^- s^{-1}$ for around 26 days. The Lomb–Scargle periodogram and its Bayesian analysis show a peak between 50 and $60 \mu\text{Hz}$ with power around $10 e^- \mu\text{Hz}^{-1} s^{-2}$ (see Figure 2(a)). From these peak profile parameters a period of 4.7816 ± 0.0015 hr (i.e., corresponding to the reported orbital period) is obtained. The Q -value for this peak profile is 174.57 with 19.22% of flux photons responsible for the orbital modulation. The goodness of fit is 2.17(40). No other signature of periodicity is observed in the PDSs. The continuum part before and after the orbital period is fitted with power-law models. The power-law index of the lower-frequency part is $\Gamma_1 = 0.65 \pm 0.14$ and higher-frequency part is $\Gamma_2 = 1.2 \pm 0.05$.

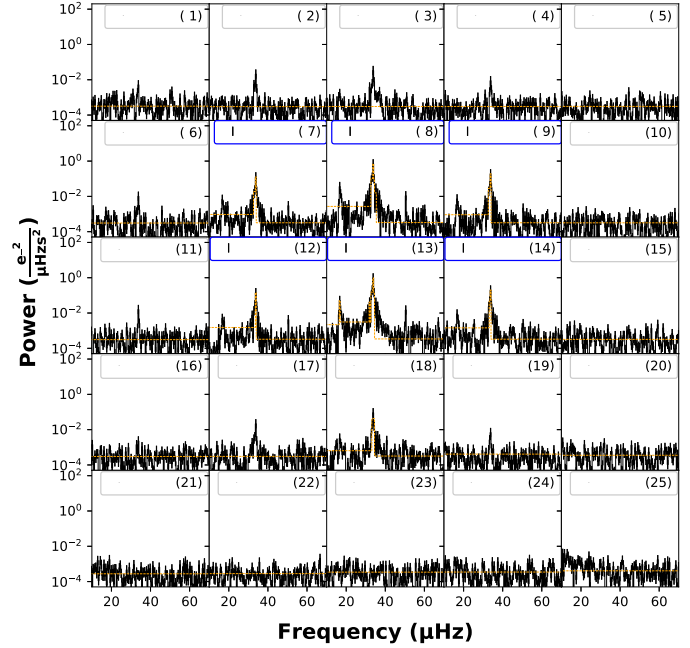
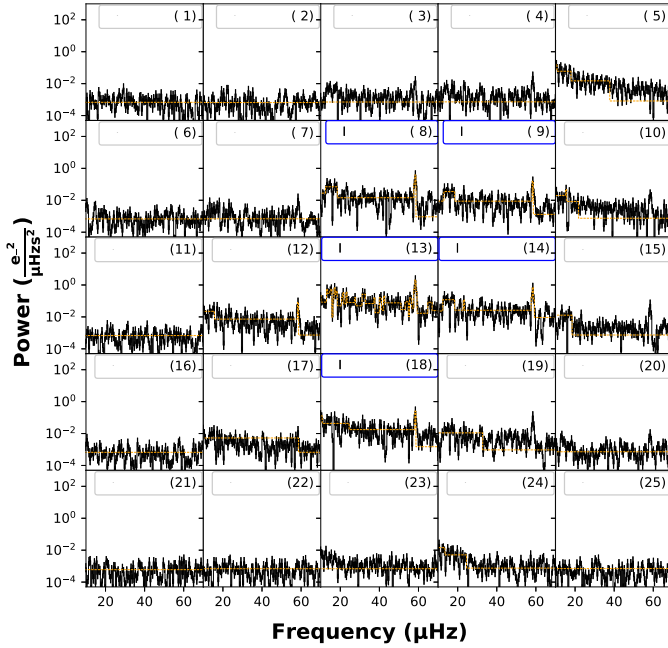
Short-time flares are also seen, and are occurring as often as that reported in Kennedy et al. (2018), Pappitto et al. (2019).

4.2. 3FGL J0523.3–2528

Figure 2(b) shows the light curve of 3FGL J0523.3–2528. TESS has observed 3FGL J0523.3–2528 for a total of 50 days in two consecutive observation sectors (#5 and #6). We checked the full-frame images, finding that different pipeline-defined aperture masks are used during two sectors. To maintain consistency, we use here the aperture mask defined by the pipeline for sector #5 for both sectors. The Lomb–Scargle periodogram and its Bayesian analysis show three peak profiles. The fundamental frequency, shown in the red dashed line, is observed at $33.56 \mu\text{Hz}$, which represents a period of 8.28 hr with a Q -value of 400.62 and 8.99% of observed flux photons responsible for the orbital motion. Around $16.89 \mu\text{Hz}$, the blue dashed line, the half-harmonic is observed, which yields an oscillation of 16.44 hr with a Q -value 165.42 and

PSR J1023+0038

3FGL J0523.3-2528

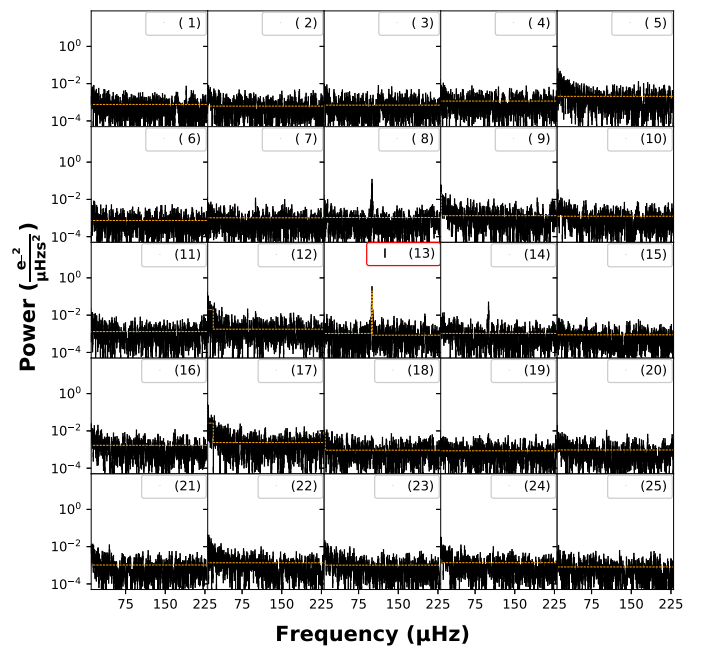
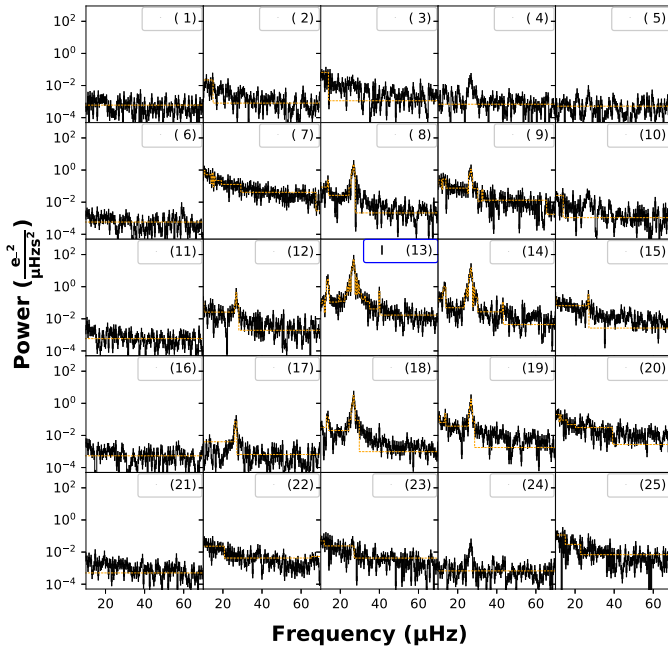


(a): Pixel-wise PDS of PSR J1023+0038

(b): Pixel-wise PDS of 3FGL J0523.3-2528

3FGL J0212.1+5320

3FGL J0744.1-2523



(c): Pixel-wise PDS of 3FGL J0212.1+5320

(d): Pixel-wise PDS of 3FGL J0744.1-2523

Figure 1. Pixel-wise power density spectra (black) along with Bayesian blocks (orange) from the pixels around the aperture mask. Blue boxes represent the pipeline-defined aperture mask. Red box represents a manually chosen aperture mask with the strongest peak profile.

2.68% observed flux involved in it. The goodness of fit is 0.12 (19). The first harmonic of this orbital motion is also observed in the PDS at $67.26 \mu\text{Hz}$. This peak is less than 95% statistically significant. This peak is ignored. Another peak profile is observed at $50.48 \mu\text{Hz}$ shown in the green dashed

line. This peak profile represents another orbital motion for 5.5 hr with a 219.18 Q -value and 3.02% rms amplitude. The continuum at a lower frequency shows a power-law index of $\Gamma_1 = 0.02 \pm 0.9$ and higher frequency shows $\Gamma_2 = 0.21 \pm 0.03$.

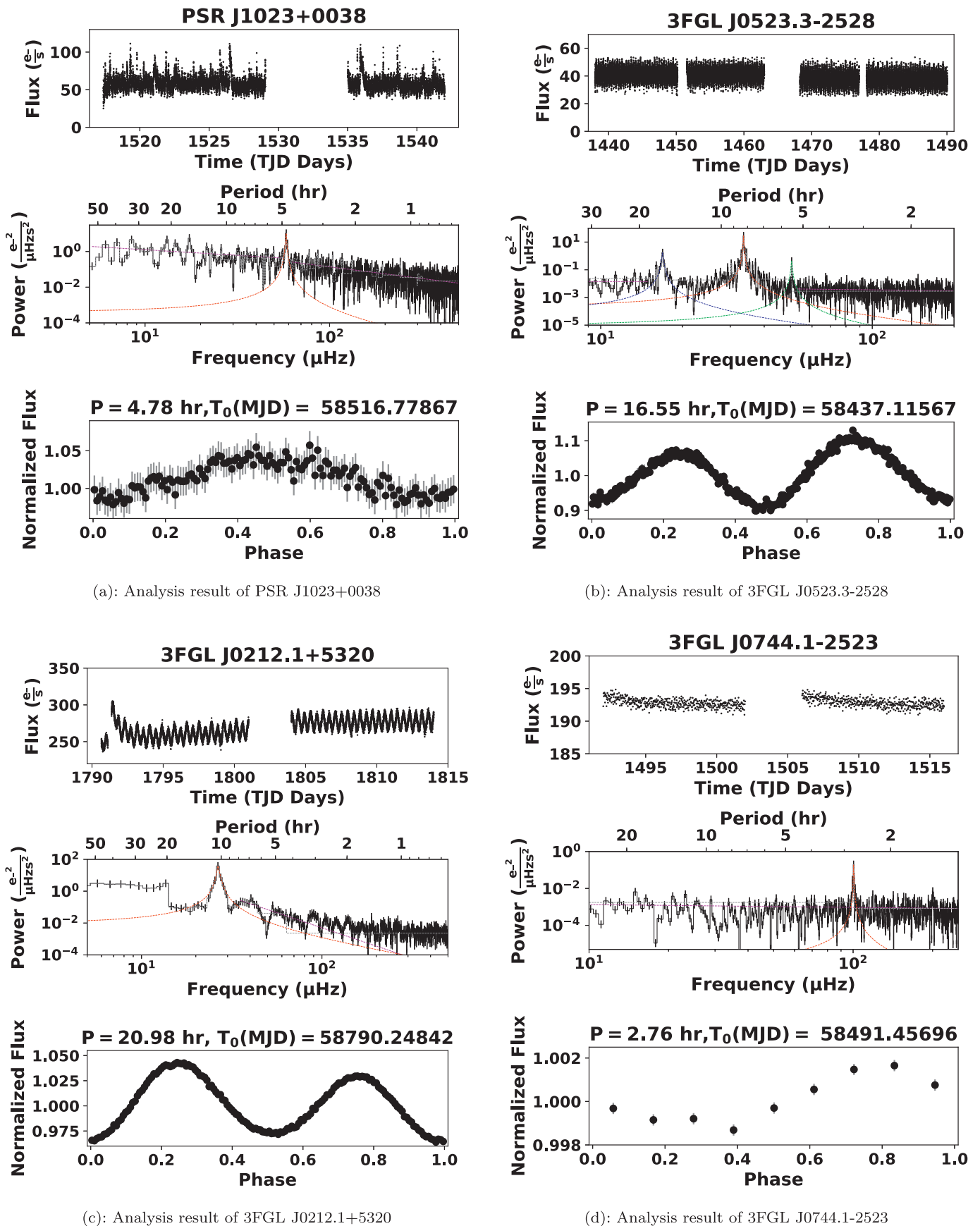
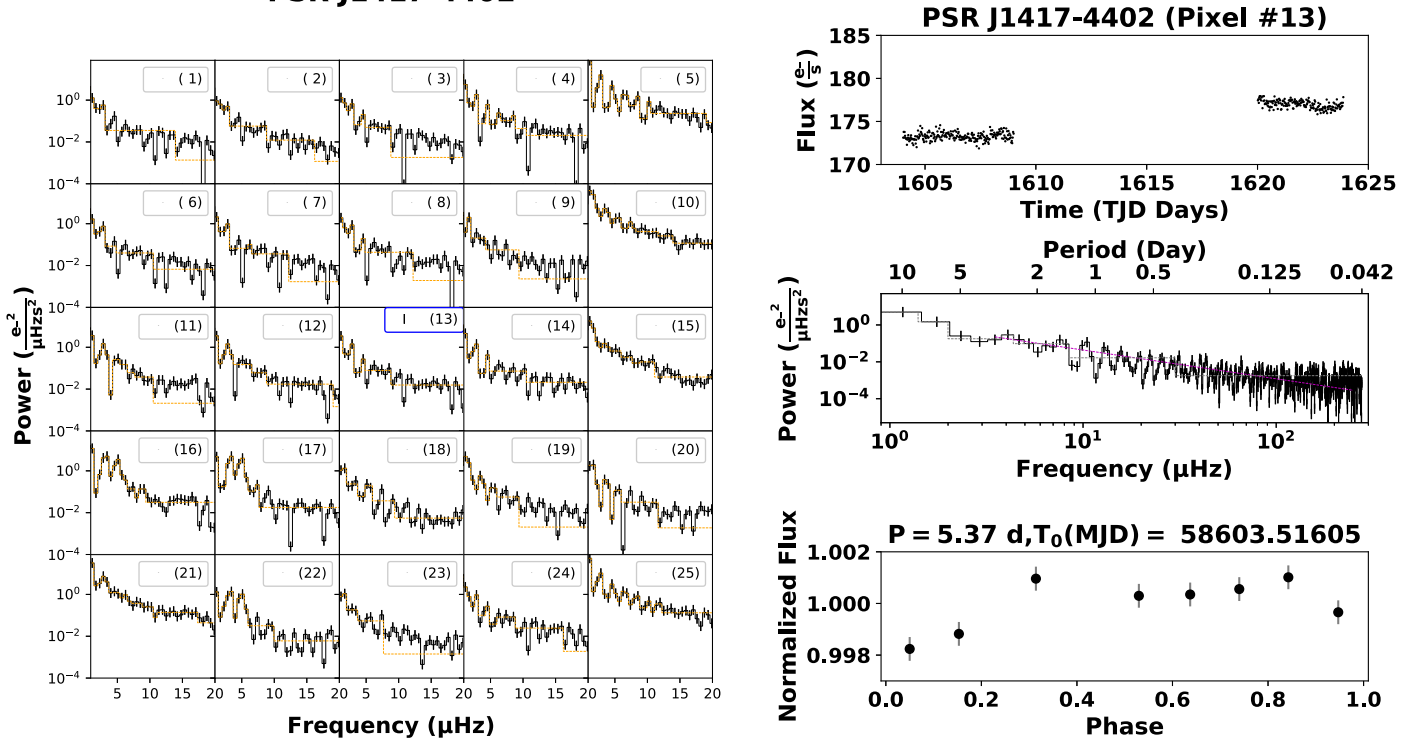


Figure 2. In all plots, the top panel shows the unbinned TESS flux light curve; the middle panel shows fitted PDSs with Bayesian blocks and peak profiles; the bottom panel shows the TESS light curves folded with periods shown above the panel.

PSR J1417-4402



(a): Pixel-wise PDS of PSR J1417-4402

(b): Analysis result of PSR J1417-4402

Figure 3. Pixel-wise power density spectra (black) along with Bayesian blocks (orange), around the sky region of PSR J1417–4402. The sky location of PSR J1417–4402 superimposes on pixel #13 (marked with blue). TESSCUT data from pixel #13 are further analyzed.

TESS data reveal the orbital period (16.5 hr; Strader et al. 2014) and also a period of 8.27 hr (one-half of the orbital period), which are characteristic of ellipsoidal variation (EV). In the TESS PDSs another periodicity of 5.5 hr is obtained with a significant Q -value and rms. This periodicity may represent some periodicity in the 3FGL J0523.3–2528 system that has not been reported before. Around 4.14 hr (i.e., $67 \mu\text{Hz}$) another peak may be seen that is likely a harmonic of the EV frequency. This peak profile is below the 95% Bayesian block significance.

4.3. 3FGL J0212.1+5320

Figure 2(c) shows the light curve of 3FGL J0212.1+5320. This light curve is affected by background scattering⁵ and so we select those parts of the data without severe scattering. Between TJD 1790–1795 a flare up to $300 e^- s^{-1}$ is observed, after that the flux increases gradually. We believe such an increase is genuine as we also observe changes in the phase profile as the brightness changes (but not during the “steady flux” state seen after TJD 1803). Bayesian block analysis of the PDSs shows a peak profile around $26.53 \mu\text{Hz}$. This represents a period of 10.47 hr with a 625.48 Q -value and 15.74% flux contribution for the orbital motion. The continuum at higher frequency shows a power-law index of $\Gamma = 2.34 \pm 0.10$.

This value is about twice that of the orbital period of 0.87 days, or 20.88 hr (Li et al. 2016; Linares et al. 2017). In the TESS PDS pulse profile, no peak is located around 20.88 hr/ $13.3 \mu\text{Hz}$. However, a break in frequency domain is observed

around this frequency which may cover a possible periodicity here.

4.4. 3FGL J0744.1–2523

In Figure 2(d) the analysis result of 3FGL J0744.1–2523 sector #7 TESSCUT data is shown. The flux rate is within $190 e^- s^{-1}$ and $195 e^- s^{-1}$ for this observation. No strong flares are observed. Here in the PDSs a pulse profile is observed from Bayesian block analysis. At $100.52 \mu\text{Hz}$ one peak profile is observed, shown in red color. This peak represents a 2.76 hr period with a Q -value = 815.86 and rms = 0.7%. The flat continuum of PDSs shows a power-law index of $\Gamma = 0.15 \pm 0.14$.

4.5. PSR J1417–4402

In Figure 3(a) a pixel-wise PDS diagram for PSR J1417–4402 is shown where no significant periodicity can be seen. Pixel #13 is analyzed and shown in Figure 3(b). We folded the light curve with the reported orbital period 5.37372(3) days (Camilo et al. 2016), corresponding to a frequency $2.15 \mu\text{Hz}$, as shown in Figure 3(c). The uneven binning in the folded light curve is due to the time gap in the light curve.

5. Discussion

The orbital period PSR J1023+0038 obtained in this work is formally not the same as reported earlier. A caveat in this work is that we did not exclude the flares from the original light curve, and so the flaring signals may contaminate the periodic signal. Since this work is mainly to demonstrate the capability of TESS to search for periodicities from a large sample of

⁵ https://tasoc.dk/docs/release_notes/tess_sector_18_drm25_v01.pdf

sources, we did not attempt to remove the flares, as has been done in Kennedy et al. (2018) and Papitto et al. (2019) for the K2 80-day light curve with a 58.8 s cadence.

Two peaks resulting from the secondary star's ellipsoidal modulation can be seen in the orbital phased light curves of 3FGL J0523.3–2528 and 3FGL J0212.1+5320 (see the bottom panels of Figures 2(b)–(c)). Other than the two maxima and minima consistent with previous observations (Strader et al. 2014; Li et al. 2016; Linares et al. 2017), we find asymmetries in both the minima and maxima. It confirms the findings of Li et al. (2016) and Linares et al. (2017) for 3FGL J0212.1+5320, and the asymmetry is first discovered for 3FGL J0523.3–2528 (whereas in previously reported light curves no significant asymmetry can be seen between the two maxima due to lower photometric accuracy; Strader et al. 2014). While the unequal minima might be partly explained by limb- and gravity-darkening effects, the unequal maxima distinguish these two pulsar binaries from normal ellipsoidal variables. Various models based on additional light sources have been proposed to explain this phenomenon, such as off-center heating from an intra-binary shock (Romani & Sanchez 2016) or starspot activity (van Staden & Antoniadis 2016).

For 3FGL J0212.1+5320, one may compare the EV-derived orbital period seen in TESS data (20.9318 ± 0.0102 hr, taken around the mean MJD 58802) with that reported earlier in Li et al. (2016; 20.8698(1) hr taken at a mean MJD 57357) and Linares et al. (2017; 20.8692(36) hr, taken at a mean MJD 57218), showing a plausible hint of increasing orbital period over time, but caution must be taken not to overinterpret such a possibility.

For 3FGL J0744.1–2523, an optical period of 2.7701 ± 0.0012 hr is reported in Salvetti et al. (2017). The periodicity value 2.76342 ± 0.00079 obtained from our analysis is comparable with the literature value.

In the case of PSR J1417–4402 there is a flux gap within the light curve. Here we focus on periodicity analysis. The orbital period of PSR J1417–4402 is reported to be around 5.37372 (3) days (Camilo et al. 2016). The effective exposure of the data analyzed is around 10 days, a mere two orbital cycles. Combined with the flux gap and contamination from a nearby bright star, it may explain the nondetection of the period.

6. Conclusions

In this Letter, TESS data from five pulsar binaries (or candidates thereof) are analyzed. In two cases (i.e., PSR J1023+0038 and 3FGL J0744.1–2523) the period can be identified with the orbital period itself where the optical brightness variation may be due to pulsar irradiation. For two other cases (i.e., 3FGL J0523.3–2528, 3FGL J0212.1+5320), frequency peaks corresponding to literature values can be obtained and optical modulations are observed at half the orbital period values, which are EV signatures.

In summary, TESS data revealed periodicities seen in four previously reported redback-like systems. Analysis of TESS data for other similar binary systems will explore more information.


P.S.P. acknowledges SYSU-Postdoctoral Fellowship. P.S.P. and P.H.T. are supported by NSFC through grants 11633007, 11661161010, and U1731136. K.L.L. is supported by the Ministry of Science and Technology (MOST) of the Republic

of China (Taiwan) through grant 108-2112-M-007-025-MY3. C.Y.H. is supported by the National Research Foundation of Korea through grants 2016R1A5A1013277 and 2019R1F1A1062071. A.K.H.K. is supported by MOST of the Republic of China (Taiwan) through grant 105-2119-M-007-028-MY3. We thank the Science Processing Operations Center (SPOC-NASA) and Mikulski Archive for Space Telescopes (MAST-STScI) for archival of the TESS data.

Facility: TESS (Ricker et al. 2015).

Software: Astropy (v3.2.1 Astropy Collaboration et al. 2013), Astroquery (Ginsburg et al. 2013), v0.3.10, SciPy (v1.2.1 Virtanen et al. 2019), Lightkurve (v1.6 Lightkurve Collaboration et al. 2018), NumPy (v1.17.3 van der Walt et al. 2011).

ORCID iDs

Partha Sarathi Pal  <https://orcid.org/0000-0001-8922-8391>
 P. H. T. Tam  <https://orcid.org/0000-0002-1262-7375>
 K. L. Li  <https://orcid.org/0000-0002-0439-7047>
 C. Y. Hui  <https://orcid.org/0000-0003-1753-1660>
 A. K. H. Kong  <https://orcid.org/0000-0002-5105-344X>

References

- Abdo, A. A., Ackermann, M., Ajello, M., et al. 2010, *ApJS*, **188**, 405
 Acero, F., Ackermann, M., Ajello, M., et al. 2015, *ApJS*, **218**, 23
 Archibald, A. M., Stairs, I. H., Ransom, S. M., et al. 2009, *Sci*, **324**, 1411
 Astropy Collaboration, Robitaille, T. P., Tollerud, E. J., et al. 2013, *A&A*, **558**, A33
 Balona, L. A., & Ozuyar, D. 2020, *MNRAS*, **493**, 2528
 Bassa, C. G., Patruno, A., Hessels, J. W. T., et al. 2014, *MNRAS*, **441**, 1825
 Belloni, T., Psaltis, D., & van der Klis, M. 2002, *ApJ*, **572**, 392
 Camilo, F., Reynolds, J. E., Ransom, S. M., et al. 2016, *ApJ*, **820**, 6
 Casella, P., Belloni, T., & Stella, L. 2005, *ApJ*, **629**, 403
 De Vito, M. A., Horvath, J. E., & Benvenuto, O. G. 2019, *MNRAS*, **483**, 4495
 Deller, A. T., Archibald, A. M., Brisken, W. F., et al. 2012, *ApJL*, **756**, L25
 Dorn-Wallenstein, T. Z., Levesque, E. M., & Davenport, J. R. A. 2019, *ApJ*, **878**, 155
 Ginsburg, A., Robitaille, T., Parikh, M., et al. 2013, Astroquery, doi:10.6084/m9.figshare.805208.v2
 Guillemot, L., Freire, P. C. C., Cognard, I., et al. 2012, *MNRAS*, **422**, 1294
 Hui, C. Y., & Li, K. L. 2019, *Galax*, **7**, 93
 Kennedy, M. R., Clark, C. J., Voisin, G., & Breton, R. P. 2018, *MNRAS*, **477**, 1120
 Li, K.-L., Kong, A. K. H., Hou, X., et al. 2016, *ApJ*, **833**, 143
 Lightkurve Collaboration, Cardoso, J. V. d. M., Hedges, C., et al. 2018, Lightkurve: Kepler and TESS Time Series Analysis in Python, Astrophysics Source Code Library, ascl:1812.013
 Linares, M. 2018, *MNRAS*, **473**, L50
 Linares, M., Miles-Páez, P., Rodríguez-Gil, P., et al. 2017, *MNRAS*, **465**, 4602
 McConnell, O., Callanan, P. J., Kennedy, M., et al. 2015, *MNRAS*, **451**, 3468
 Papitto, A., Ambrosino, F., Stella, L., et al. 2019, *ApJ*, **882**, 104
 Papitto, A., Ferrigno, C., Bozzo, E., et al. 2013, *Natur*, **501**, 517
 Patruno, A., Archibald, A. M., Hessels, J. W. T., et al. 2014, *ApJL*, **781**, L3
 Petrov, L., Mahony, E. K., Edwards, P. G., et al. 2013, *MNRAS*, **432**, 1294
 Ricker, G. R., Winn, J. N., Vanderspek, R., et al. 2015, *JATIS*, **1**, 014003
 Roberts, M. S. E. 2013, in IAU Symp. 291, Neutron Stars and Pulsars: Challenges and Opportunities after 80 Years, ed. J. van Leeuwen (Cambridge: Cambridge Univ. Press), 127
 Romani, R. W., & Sanchez, N. 2016, *ApJ*, **828**, 7
 Roy, J., Ray, P. S., Bhattacharyya, B., et al. 2015, *ApJL*, **800**, L12
 Salvetti, D., Mignani, R. P., De Luca, A., et al. 2017, *MNRAS*, **470**, 466
 Scargle, J. D., Norris, J. P., Jackson, B., & Chiang, J. 2013, *ApJ*, **764**, 167
 Shahbaz, T., Linares, M., & Breton, R. P. 2017, *MNRAS*, **472**, 4287
 Shahbaz, T., Linares, M., Rodríguez-Gil, P., & Casares, J. 2019, *MNRAS*, **488**, 198
 Stappers, B. W., Archibald, A. M., Hessels, J. W. T., et al. 2014, *ApJ*, **790**, 39
 Strader, J., Chomiuk, L., Cheung, C. C., et al. 2015, *ApJL*, **804**, L12
 Strader, J., Chomiuk, L., Sonbas, E., et al. 2014, *ApJL*, **788**, L27
 Swihart, S. J., Strader, J., Chomiuk, L., & Shishkovsky, L. 2019, *ApJ*, **876**, 8
 Swihart, S. J., Strader, J., Shishkovsky, L., et al. 2018, *ApJ*, **866**, 83

Szkody, P., Fraser, O., Silvestri, N., et al. 2003, [AJ](#), **126**, 1499
Takata, J., Li, K. L., Leung, G. C. K., et al. 2014, [ApJ](#), **785**, 131
Tam, P. H. T., Hui, C. Y., Huang, R. H. H., et al. 2010, [ApJL](#), **724**, L207
Thorstensen, J. R., & Armstrong, E. 2005, [AJ](#), **130**, 759
van der Walt, S., Colbert, S. C., & Varoquaux, G. 2011, [CSE](#), **13**, 22

van Staden, A. D., & Antoniadis, J. 2016, [ApJL](#), **833**, L12
Virtanen, P., Gommers, R., Burovski, E., et al. 2019, scipy/scipy: SciPy 1.2.1, v1.2.1, Zenodo, doi:[10.5281/zenodo.2560881](#)
Woudt, P. A., Warner, B., & Pretorius, M. L. 2004, [MNRAS](#), **351**, 1015